Structural, magnetic and transport properties of $La_{0.8}Sr_{0.2}MnO_3/xNiO$ composites

2006 J. Phys.: Condens. Matter 18 8281

(http://iopscience.iop.org/0953-8984/18/35/014)

INSTITUTE OF PHYSICS PUBLISHING JOURNAL OF PHYSICS: CONDENSED MATTER

J. Phys.: Condens. Matter **18** (2006) 8281–8294 doi:10.1088/0953-8984/18/35/014

Structural, magnetic and transport properties of $La_{0.8}Sr_{0.2}MnO_3/x$NiO composites

M Eshraghi, H Salamati[1] and P Kameli

Department of Physics, Isfahan University of Technology, Isfahan 84154, Iran

E-mail: salamati@cc.iut.ac.ir

Received 5 June 2006, in final form 30 July 2006
Published 18 August 2006
Online at stacks.iop.org/JPhysCM/18/8281

Abstract

The effect of NiO doping on the structure, magnetic and magnetotransport properties of $La_{0.8}Sr_{0.2}MnO_3$(LSMO)/xNiO has been investigated. Two types of LSMO/xNiO composites were prepared by different processes using the solid-state reaction method. In the first type, the LSMO powders are mixed with small particle size NiO (SA_x samples) and in the second type the LSMO powders are mixed with as-powder NiO (SB_x samples). These studies show that some part of the Ni goes into the perovskite lattice, substituting Mn in LSMO, and the remainder segregates as a separate phase at the grain boundaries and grain surfaces. The presence of NiO at the grain boundaries increases the number of disordered states at the surface of the grains and therefore the low-temperature resistivity increases very quickly with the increase of NiO doping level. Results also show that the NiO doping has an effect on the low-field magnetoresistance (LFMR). The value of magnetoresistance (MR) increases for a low doping level of $0 \leqslant x \leqslant 3$ and decreases at a high doping level of $x \geqslant 5$. The spin-dependent tunnelling and scattering at the interfaces of the grain boundaries are responsible for the increasing of LFMR at $x \leqslant 3$, while reduction of the LFMR at $x \geqslant 5$ originates from substitution of Ni^{2+} for the Mn^{3+} ions, which introduces magnetic dilution into the samples. Also it can be found that, as $T < 230$ K, the MR value of the SB_3 sample is larger than that of the SA_3 sample due to the presence of a larger amount of NiO at the grain boundaries and surfaces.

1. Introduction

Since the discovery of the phenomenon of colossal magnetoresistance (CMR) in the $La_{1-x}A_xMnO_3$ (A = Sr, Ca, Ba or vacancies) system, there have been extensive research activities on these doped perovskites [1–4]. Besides fundamental understanding of mechanism

[1] Author to whom any correspondence should be addressed.

of the CMR, the studies have also been motivated by the potential applications of these materials. However, the intrinsic CMR effect in the perovskite manganites, which is caused by the double exchange mechanism [5], is found on a magnetic field scale of several teslas and a narrow temperature range. Recently, the effect of grain boundaries in the perovskite manganites has been studied intensively [6–14]. It was found that the presence of grain boundaries in polycrystalline samples leads to a large low-field magnetoresistance (LFMR) effect over a wide temperature range below the Curie temperature T_c. This specific property of grain boundaries makes them attractive for applications usually requiring a large and almost temperature-independent MR effect at small applied fields. Several models have been proposed for the theoretical description of grain boundary behaviours in the perovskite manganites. Hwang *et al* [6] proposed a model based on spin-polarized tunnelling between ferromagnetic grains through an insulating grain boundary barrier. Evetts *et al* [9] proposed the polarization of the grain boundary region by adjacent magnetically soft grains. Guinea [10] pointed out that probably tunnelling occurs via paramagnetic impurity states in the grain boundary barrier. Several attempts have been made to enhance the LFMR effect of perovskite manganites by mixture of these CMR materials with secondary phases. They include LSMO/CeO_2 [15], LCMO/$SrTiO_3$ [16], LCMO/MgO [17] and LSMO/TiO_2 [18]. Although the doping effects of nonmagnetic impurities on the electrical transport of manganites have been investigated by several groups, the magnetic and magnetotransport behaviour of composites of magnetic insulator and CMR materials has rarely been investigated.

In this work, we report the structural, magnetic and magnetotransport properties of $La_{0.8}Sr_{0.2}MnO_3/x$NiO composites ($x = 0$, 1, 2, 3, 5 and 7.5 wt%). Bulk NiO has rhombohedral structure and is antiferromagnetic below 523 K, whereas it has cubic structure and is paramagnetic above that temperature [19, 20].

2. Experimental details

The $La_{0.8}Sr_{0.2}MnO_3/x$NiO samples with $x = 0$, 1, 2, 3, 5, and 7.5 wt% were prepared in two steps. First the $La_{0.8}Sr_{0.2}MnO_3$ (LSMO) powders were prepared by a conventional solid-state reaction method. High-purity powders (better than 99.9% from Merck Company) of La_2O_3, $SrCO_3$ and MnO_2 were mixed in stoichiometric proportions, calcined at 1200 °C for 24 h. The calcination and grinding procedures were repeated three times. In order to obtain very fine and homogenous samples, the resulting powders were subjected to high-energy ball milling using a planetary mill for 1 h. Two types of LSMO/xNiO composites were prepared by the following processes.

(A) The LSMO powders were mixed with small particle size NiO (these will be referred to as SA_x samples). In order to obtain small-size NiO powders, high-energy ball milling was used. The NiO high-purity powders (better than 99.9% from Merck Company) were put in a cylindrical bowl and seven 10 mm diameters agate balls were used for grinding. A rotational speed of 400 rpm was chosen and sample was ground for a period of 47 h.

(B) The LSMO powders were mixed with as powder NiO (these samples are denoted by SB_x). Appropriate amounts of LSMO and NiO powders were mixed and a homogeneous powder was formed. Finally the two different mixtures were pelletized at a pressure of 10^5 N cm^{-2} and sintered at 1250 °C for 24 h.

The resistivity measurements were carried out by the four-probe method in magnetic field range of 0–8000 Oe, using a Leybold closed-cycle refrigerator at low temperatures down to 10 K. The AC susceptibility measurements were performed using a Lake Shore AC susceptometer, Model 7000. X-ray diffraction (XRD) patterns of samples were taken on Philips

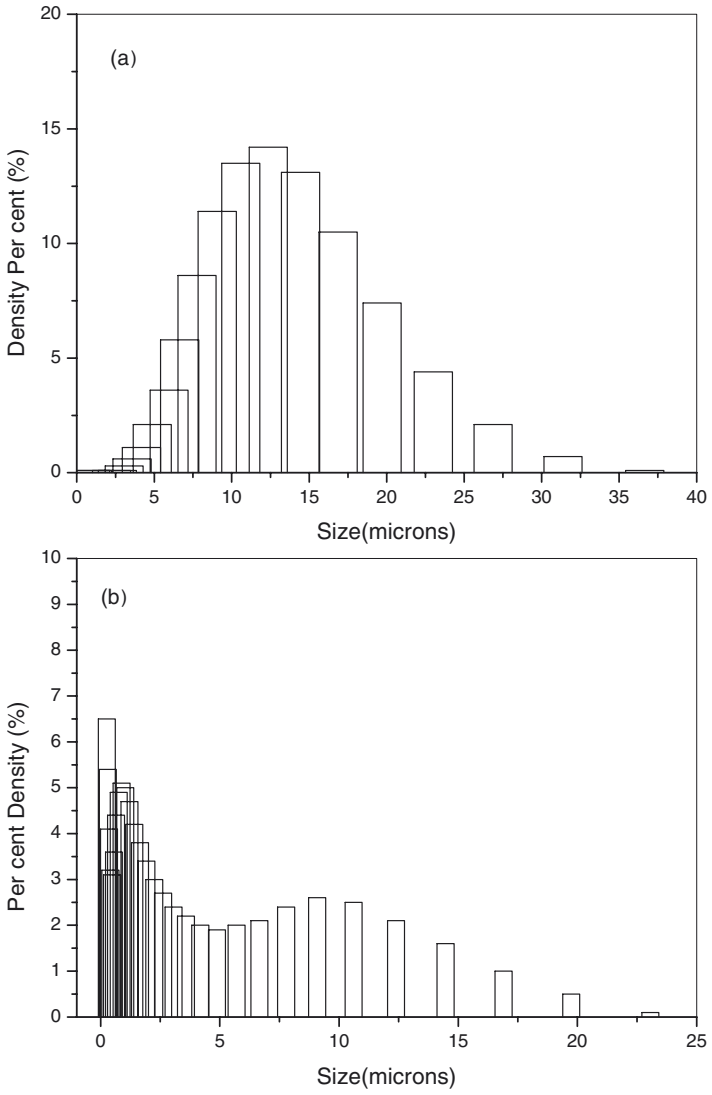

Figure 1. Histogram showing the particle size distribution of powder (a) and 47 h milled (b) samples.

XPERT x-ray diffractometer. The microstructure of samples was taken on Philips XL 30 scanning electron microscope (SEM). The particle size and the distribution of powders were analysed by a FRITSCH GmbH laser particle size analyser (LPSA).

3. Results and discussion

Figure 1 shows the size distribution for powder and 47 h milled NiO samples. The average particle sizes decreased from 13.5 to 3.5 μm after 47 h ball milling. Figure 2 shows the XRD patterns at room temperature for SA_x samples. The XRD analyses reveal that all samples have a rhombohedral structure. As one can see, at lower concentrations it is hard to see the peaks

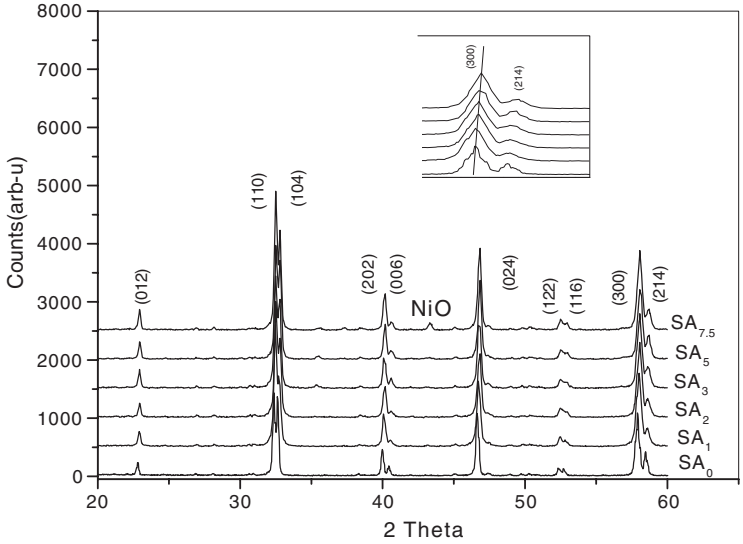

Figure 2. XRD patterns of SA_x samples. The inset depicts the evolution of the peaks (300) and (214) due to the NiO doping.

related to NiO and other impurities in composites, and LSMO lines were observed clearly. But there is a small peak observed at $2\theta \approx 43^\circ$ and at high concentrations of NiO. This peak is related to NiO in the composites, and as can be seen, the peak intensity increases by increasing x. This suggests that the NiO and LSMO are coexistent in the composites of LSMO/xNiO. However, there is observed a slight continuous shift towards higher 2θ values when x increases for all diffraction peaks (see the inset of figure 2). This result indicates a decrease in the lattice parameter from 5.50 Å for the SA_0 sample to 5.49 Å for the $SA_{7.5}$ sample. This means that some part of the Ni goes into the perovskite lattice, substituting Mn in LSMO. Due to the smaller ionic radius of Ni^{2+} compared with Mn^{3+}, the lattice parameter decreases with the increase of NiO concentration. This behaviour was observed by Pal *et al* [21] in Ni-doped $La_{0.7}Pb_{0.3}MnO_3$ samples. They investigated the role of the Ni ion in the structure, magnetic and transport properties of perovskites $La_{0.7}Pb_{0.3}Mn_{1-x}Ni_xO_3$. They found that the cell volume decreases slightly by substituting the Mn^{3+} site with Ni^{2+}. Also Their XPS analyses show that the ionic state of Ni in $La_{0.7}Pb_{0.3}Mn_{1-x}Ni_xO_3$ samples is mainly Ni^{2+}.

In order to analyse the effects of NiO on the microstructure of LSMO grains and the distribution of NiO in the composites, fracture sections of all the samples were examined by the SEM and EDX. Typical SEM micrographs of the composites (SA_0, SA_3 and $SA_{7.5}$) are shown in figure 3. As shown in figure 3(a), a relatively clearer grain boundary is observed in the pure LSMO (SA_0) sample. However, in the NiO-doped composites the NiO is present mainly at the grain boundaries and grain surfaces of LSMO, as shown in figures 3(b) and 3(c). Meanwhile, EDX analyses indicate that as x increases NiO segregates as a separate phase in the LSMO matrix, and makes the grain boundaries of the LSMO ambiguous at high doping level. As x increases, more and more Ni diffuses from the interior of the LSMO grains and gets segregated in the grain boundaries.

Figure 4 shows the temperature dependence of the real part of the AC susceptibility for SA_x samples in the AC field amplitude of 500 A m^{-1} at a frequency of 333 Hz. All samples show the paramagnetic to ferromagnetic transition. As one can see, the transition temperature

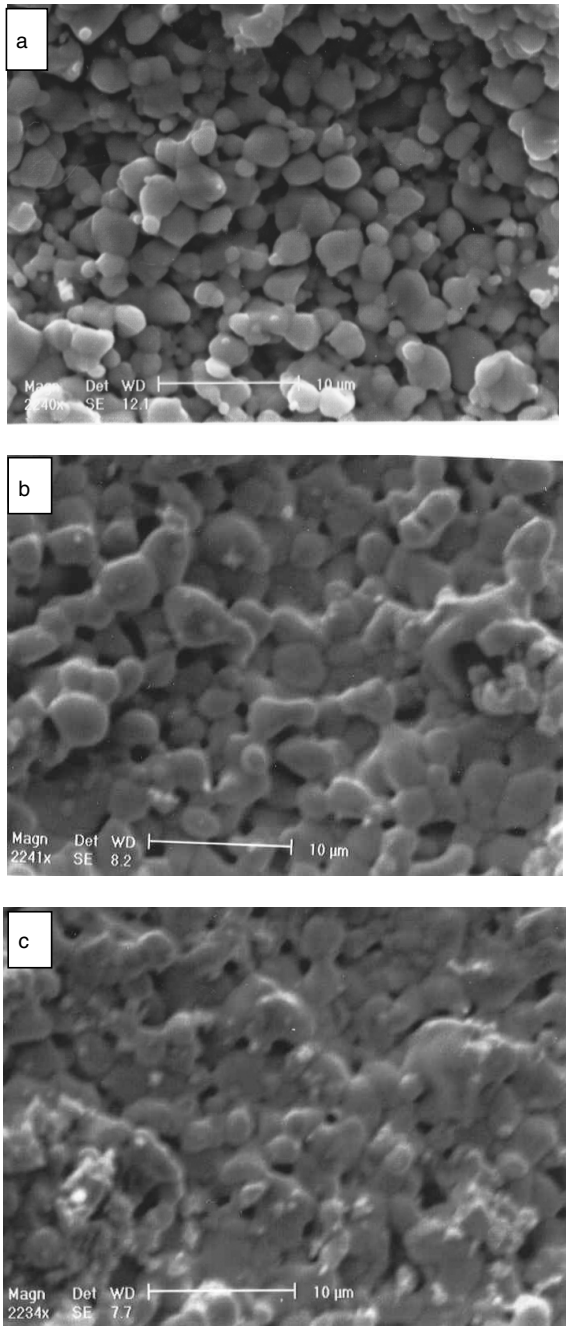

Figure 3. SEM micrographs of the composites (SA_0, SA_3 and $SA_{7.5}$).

and magnetization decrease with the increase of NiO concentration. These results show that the partial substitution of Ni^{2+} ion for the Mn^{3+} ion weakens the double exchange interaction significantly, and as a result T_c and the magnetization decrease because of magnetic dilution.

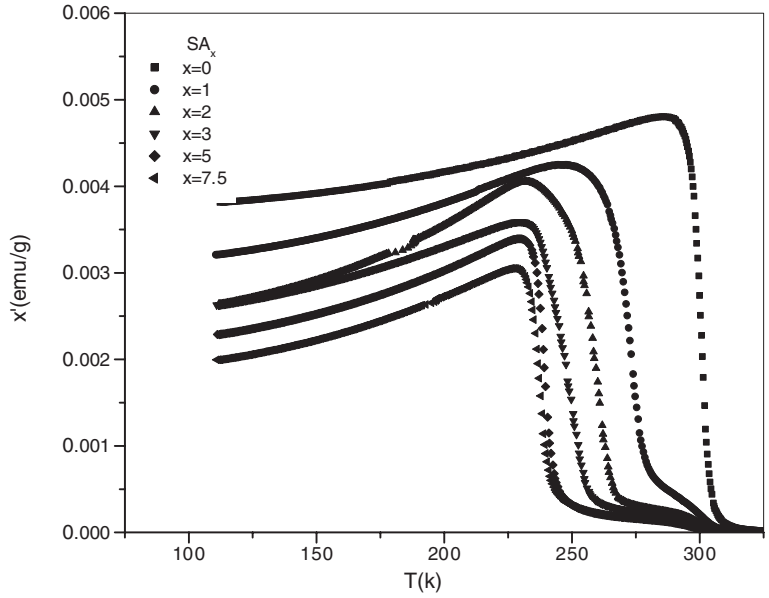

Figure 4. Temperature dependence of the real part of the AC susceptibility for SA_x samples in an AC field amplitude of 500 A m^{-1} at a frequency of 333 Hz.

One more reason for the increase of the transition width and decrease of magnetization with the increase of NiO doping level is the presence of this antiferromagnetic material at the grain boundaries and grain surfaces. The presence of NiO at the surfaces of the grains increases the number of magnetically disordered states in the surface and therefore the magnetization decreases with the increase of NiO concentration.

Figure 5(a) shows the resistivity versus temperature plot of SA_0 sample in a zero magnetic field. As one can see, there is a small peak at temperature T_{p1} which is close to the Curie temperature T_c, and a second broad peak at T_{p2} well below T_c. This kind of behaviour was seen in individual thin-film grain boundaries in perovskite manganites [22] and polycrystalline samples [13, 23, 24]. This behaviour may be explained by the model proposed by Zhang *et al* [24]. According to this model, in granular perovskite system a grain of the perovskite can be assumed as a two-phase system, a body and a surface. The body phase would have the same properties as the bulk compound (magnetic and transport properties), but the surface phase would have low transition temperature and magnetization. This is because of the magnetically disordered states in the surface. These magnetically disordered states at the grain surface are due to the high degree of (a) oxygen deficiencies, (b) breaking of Mn–O–Mn paths, (c) deviation of stoichiometric composition, (d) termination of crystal structure, and (e) dislocations. In this model T_{p1} reflects the intrinsic metal–insulator transition temperature but the resistivity peak at temperature well below T_c, (T_{p2}) does not mean a metal–insulator-like transition for the granular system and indicates the interfacial tunnelling due to the difference in magnetic order between the surface and body. The resistivity of the surface phase should decrease with increasing temperature when the surface becomes a paramagnetic state, while the body phase is still in the ferromagnetic state. As a result, the low-temperature resistivity peak appears at the surface Curie temperature T_{cs}, approximately.

Figure 5(b) shows the resistivity versus temperature plot of SA_x samples in a zero magnetic field. As one can see, T_{p1} and T_{p2} decrease with the increase of doping level x. Also an

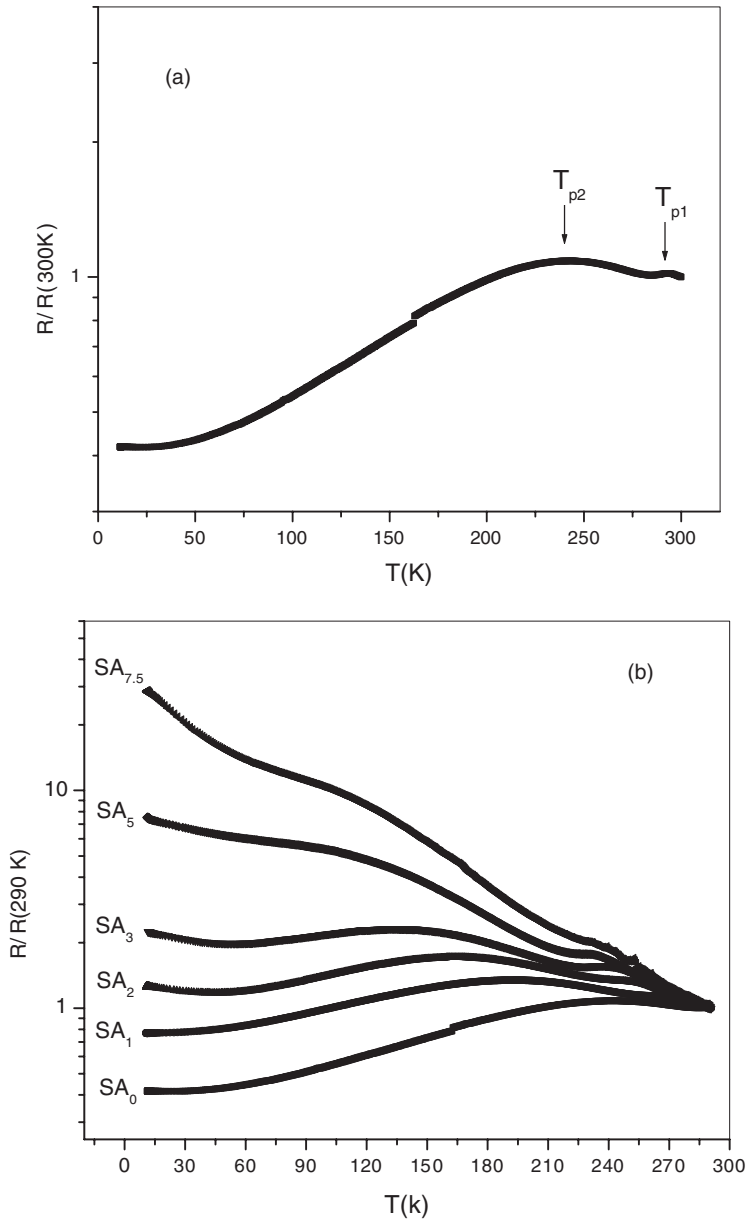

Figure 5. The resistivity versus temperature of the SA_0 sample in a zero magnetic field (a) and temperature dependence of the resistivity for SA_x samples in zero magnetic field (b).

increase in resistivity is observed due to the NiO doping of LSMO samples. As discussed in the literature [25, 26], there are two kinds of conduction channel, connected in parallel in the polycrystalline LSMO/xNiO composite samples. One is related to intragrain, and the second is related to intergrain, hopping of the conduction electrons between the neighbouring sites. Moreover, the resistance of grain boundaries is more than the resistance inside the grains because of the disordered nature of the grain boundaries. NiO doping in LSMO samples has

two different effects. In the pure LSMO samples the electrical transport is realized through a direct contact between the LSMO grains. This direct contact is diluted/disturbed as a result of the introduction of a NiO antiferromagnetic insulator. On increasing the NiO content to high concentrations, some part of the Ni goes inside the grains, substituting the Mn site in the LSMO lattice, and the remainder goes to the grain boundaries. If Ni substitutes Mn in the perovskite lattice, it cannot participate in the double-exchange (DE) mechanism involving Mn^{3+} and Mn^{4+} ions, so, in effect, it dilutes the DE process. For that reason T_{p1} decreases and the resistivity increases with the increase of the NiO doping level. Also the presence of NiO at the grain boundaries increases the number of disordered states at the surface of the grains and therefore T_{p2} decreases and the low-temperature resistivity increases very quickly with the increase of x. This behaviour has been confirmed by XRD analyses. As was mentioned, the lattice parameter increases slightly with increasing concentration of NiO. Also the intensity of the NiO peak in the XRD spectra increases with increasing NiO doping level.

In the observation of temperature dependence of the resistivity curves, an unexpected increase at low temperatures was found in the doped samples. This effect is observed in small grain size manganite and half-metallic ferromagnetic samples, and it can be related to an electrostatic blockade of carriers between grains [13, 27, 28]. The intergrain conduction mechanism arises from transport of charge carriers between grains. This requires the generation of a charge carrier by removing an electron from a neutral grain and placing it in a neighbouring hitherto neutral grain at the expense of the electrostatic charging energy E_c. At low temperatures and for small grains, it is increasingly difficult to activate this mechanism. In this situation, transport can be effectively blocked, giving as a result an upturn in the low-temperature resistivity. This is the so-called Coulomb blockade. As discussed before, in the case of NiO-doped samples, with the increase of NiO doping, the magnetically disordered surface layer of the grains increases, and on the other hand the surface-to-volume ratio increases. So the effective grain size decreases with increasing NiO concentration. The Coulomb blockade model predicts a temperature dependence for the resistivity in the form [29, 30]

$$\rho(T) = \rho(0)\exp(\sqrt{C/T}). \tag{1}$$

This functional form can be observed in the fits of figure 6(a). The slope of those lines (C) is proportional to the electrostatic blocking energy, E_c. As we can see in figure 6(b), C increases with the increase of NiO doping level x. This indicates the increasing influence of the barrier between grains with increasing NiO concentration at the grain boundaries.

Before concluding this section, we would like to mention the existence of double peaks of another type in polycrystalline samples prepared by different methods. Gelbert *et al* [31] have shown that chemical inhomogeneity is the origin of the double peak in the resistivity behaviour of their samples. Sun *et al* [32] have shown that the oxygenation inhomogeneity leads to a double-peak behaviour. In these cases, the compositional disorder occurs on the scale of the whole sample and not in each grain as in the case of small grain size samples. Araujo-Moreira *et al* [33] have shown that in the case of an LCMO thin film with such a chemical inhomogeneity, several peaks are present in the imaginary component of the AC susceptibility. The AC susceptibility behaviour of our SA_x samples (shown in figure 7 for $x = 0.0$ and 7.5) confirms that no macroscopic inhomogeneity is present, despite the double-peak behaviour of the temperature dependence of the electrical resistance.

In order to see the effect of NiO particle size on the structural, magnetic and transport properties of LSMO/xNiO composites, we will turn our attention to some experimental results. The XRD patterns of SA_3 and SB_3 samples are shown in figure 8. Both samples have the same XRD pattern with the rhombohedral crystal structure. However, it can be seen that there is a

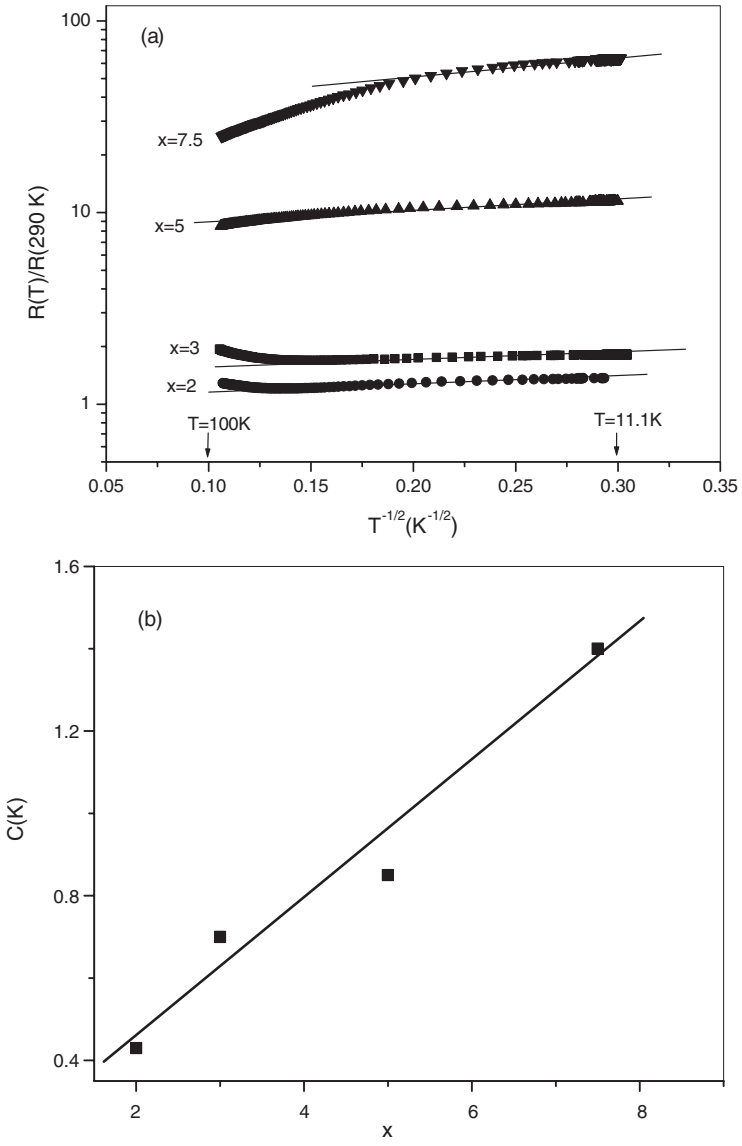

Figure 6. Reduced resistivity versus $T^{-1/2}$ for SA_x samples ($x = 2$, 3, 5 and 7.5) (a) and variation of the parameter C with the NiO doping level x (b).

slightly shift towards higher 2θ values in the XRD pattern of the SA_3 sample compared to the SB_3 sample (see the inset of figure 8). As discussed before, due to the substitution of Ni^{2+} at the Mn^{3+} site in the LSMO lattice, the lattice parameter decreases and the XRD peaks shift to higher 2θ values. So we can speculate that the amount of Ni substitution into the Mn site in the SA_3 sample is more than in the SB_3 sample. It seems that for the SA_x samples, the NiO small size particles can cover more of the surface of the LSMO grains and therefore NiO can react better with LSMO and Ni diffuses more into the LSMO grains and substitutes in the Mn site.

Figure 9 shows the temperature dependence of the real part of the AC susceptibility for SA_3 and SB_3 samples in an AC field amplitude of 500 A m^{-1} at a frequency of 333 Hz. As

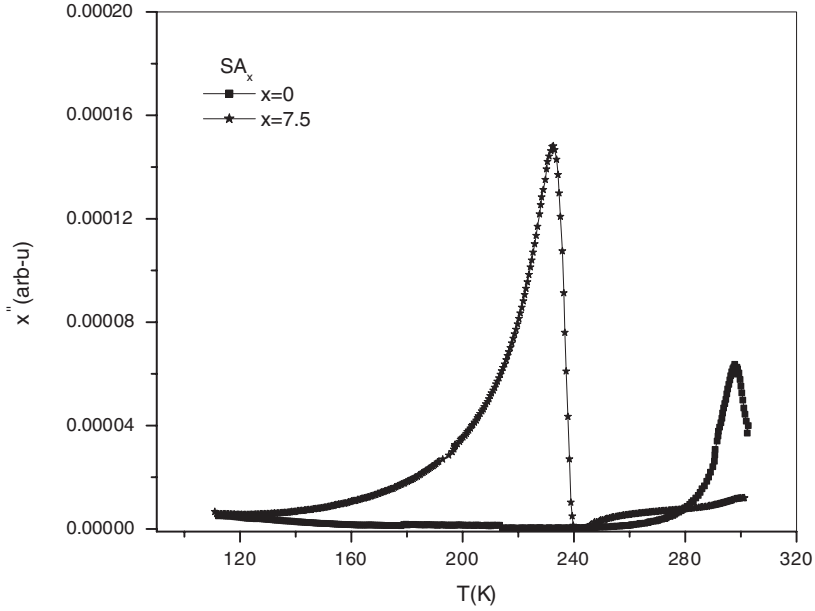

Figure 7. Temperature dependence of the imaginary part of the AC susceptibility for SA_x samples ($x = 0.0$ and 7.5) in an AC field amplitude of 500 A m^{-1} at a frequency of 333 Hz.

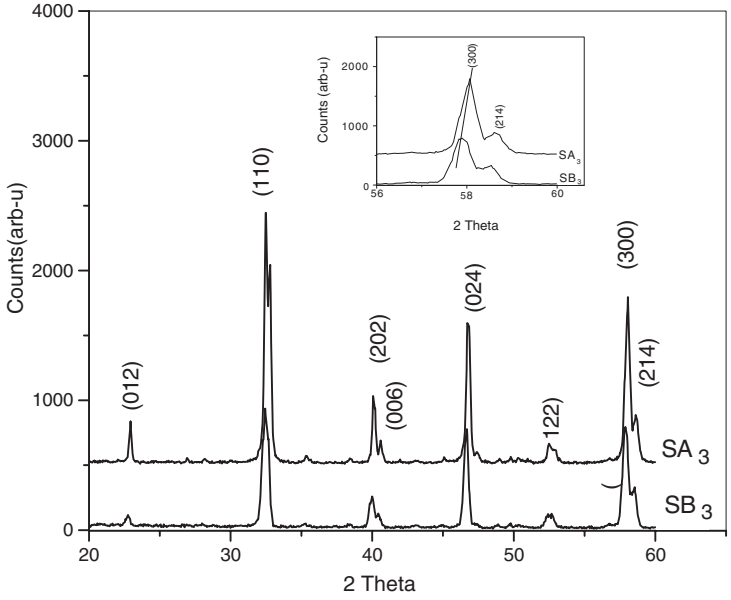

Figure 8. XRD patterns of SA_3 and SB_3 samples. The inset depicts the evolution of the peaks (300) and (214).

one can see, the transition temperature and magnetization of SA_3 sample are less than those of the SB_3 sample. This result shows that the larger amount of substitution of Ni^{2+} for Mn^{3+} in the SA_3 sample compared to the SB_3 sample leads to a higher decrease of the transition temperature and magnetization in this sample.

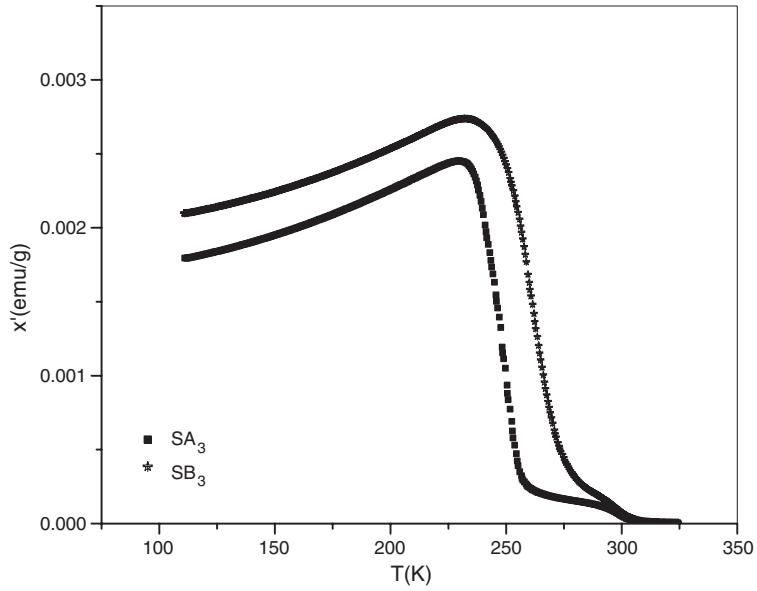

Figure 9. Temperature dependence of the real part of the AC susceptibility for SA_3 and SB_3 samples in an AC field amplitude of 500 A m^{-1} at a frequency of 333 Hz.

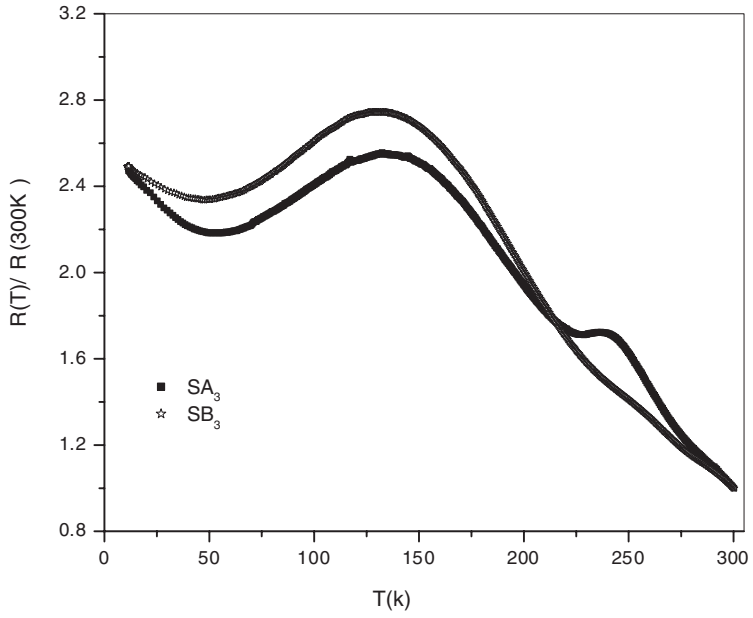

Figure 10. The resistivity versus temperature plot of SA_3 and SB_3 samples in zero magnetic field.

Figure 10 shows the temperature dependence of the resistivity for SA_3 and SB_3 samples in zero magnetic fields. Comparing to the resistivity curves for SA_3 and SB_3 samples, two different behaviours can be found, as follows. (1) the transition temperature T_{p1} for the SA_3 sample is lower than that for the SB_3 sample (235 K for SA_3 and 255 K for SB_3), but in contrast

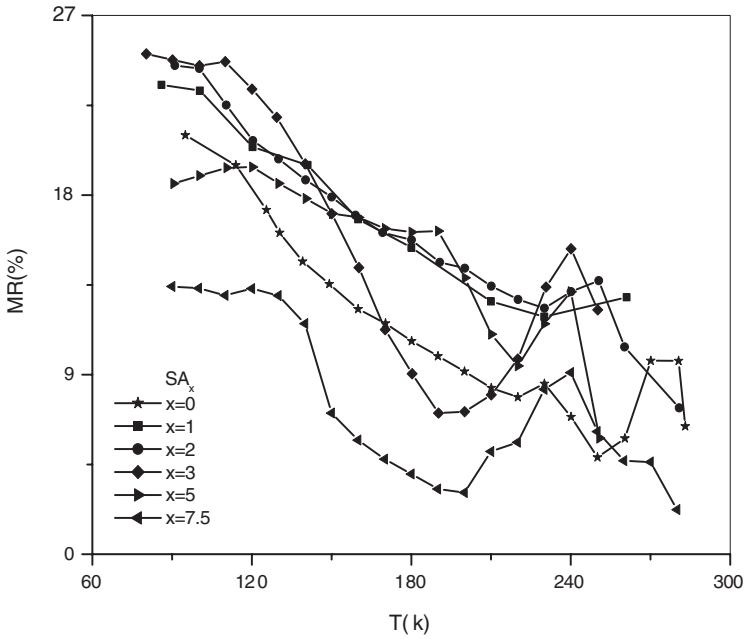

Figure 11. Temperature dependence of the MR for SA_x samples, in a magnetic field of 5000 G.

the temperature T_{p2} for the SA_3 sample is slightly higher than that for the SB_3 sample (135 K for SA_3 and 130 K for SB_3). (2) The peak at T_{p1} has almost disappeared for the SB_3 sample compared to the SA_3 sample. Also, the resistivity of the SB_3 sample is less than that of the SA_3 sample at high temperatures and higher at low temperatures. As mentioned before, in SA_x samples, due to the higher reaction rate of small particle size NiO with LSMO particles, Ni is better substituted into the Mn site and less segregated at the grain boundaries compared to the SB_x samples which are doped with powder NiO. So the effect of more Ni substitution in the SA_3 sample leads to the higher reduction of T_{p1} and increasing resistivity at high temperatures. On the other hand, due to the presence of a large amount of NiO at the grain boundaries and surfaces in the SB_3 sample, the effect of the grain boundary is more pronounced in this sample. Therefore the low-temperature resistivity is higher for the SB_3 sample compared to the SA_3 sample.

Figure 11 shows the temperature dependence of the MR for SA_x samples in a magnetic field of 5000 G. It can be seen that the value of the MR increases for a low doping level of $0 \leqslant x \leqslant 3$ and decreases at a high doping level of $x \geqslant 5$. Usually, the enhancement of LFMR is a characteristic of polycrystalline samples [6]. It originates from the spin-dependent tunnelling and scattering process at the interfaces of the grains. Hence an artificial grain boundary effect can be realized by proper incorporation of dopant into manganites. The structurally disordered interfaces play the role of an energy barrier for carriers. The tunnelling process related to the relative misorientation of the magnetization in the grains at each side of the grain boundaries should occur when the carriers pass through the interfaces of the grains. Because of the small coercive force for the manganites, the alignment process of magnetization in each grain to the applied magnetic field can occur in the low-field region. The enhancement of LFMR in NiO-doped samples closely relates to the improvement of the disordered state at the grain boundaries. Therefore the low-doped samples have a larger LFMR than the pure LSMO

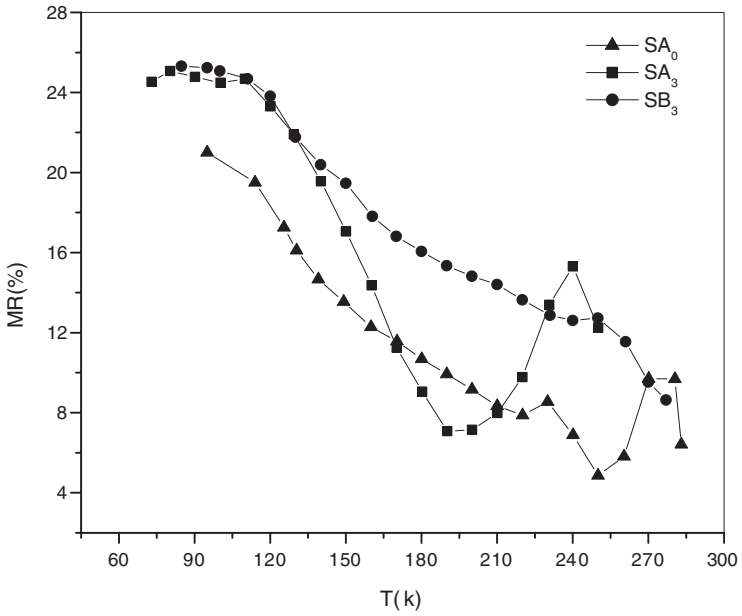

Figure 12. Temperature dependence of the MR for SA_0, SA_3 and SB_3, in a magnetic field of 5000 G.

sample, and the LFMR effect increases with increasing content of NiO. For higher amounts of NiO, due to the larger amount of the substitution of Ni^{2+} for Mn^{3+}, the mobility of charge carriers reduces (since the DE is weakened). This reduction of carrier concentration leads to an increase in resistivity and decrease in MR for the high doping level of $x \geqslant 5$. The other reason for decreases of LFMR at a high doping level may result from the grain boundary becoming too thick for electron tunnelling.

Figure 12 shows the temperature dependence of the MR for SA_0, SA_3 and SB_3 samples in a magnetic field of 5000 G. It can be seen that the MR value of the pure sample (SA_0) is less than that of SA_3 and SB_3 samples. Also comparing to the MR curves for SA_3 and SB_3 samples, it can be found that, when $T < 230$ K, the MR value of the SB_3 sample is larger than that of the SA_3 sample. As mentioned before, due to the presence of a larger amount of NiO at the grain boundaries and surfaces of the SB_3 sample, the effect of the grain boundary is more pronounced in this sample and the number of disordered states at the grain boundaries is greater for this sample. Therefore the LFMR effect increases in these samples.

4. Conclusions

NiO-doped LSMO composites were prepared by a conventional solid-state reaction method. Two types of LSMO/xNiO composite, denoted SA_x and SB_x samples, were prepared by different processes using the solid-state reaction method. These studies show that some part of the Ni goes into the perovskite lattice, substituting the Mn site in LSMO, and the remainder segregates as a separate phase at the grain boundaries and grain surfaces. The presence of NiO at the grain boundaries increases the number of disordered states at the surface of the grains and therefore the resistivity increases with the increase of NiO doping level. The results also show that the NiO doping has an effect on the LFMR. The value of MR increases for a

low doping level of $0 \leqslant x \leqslant 3$ and decreases at a high doping level of $x \geqslant 5$. The spin-dependent tunnelling and scattering at the interfaces of the grain boundaries are responsible for the increasing of the LFMR at $x \leqslant 3$, while reduction of the LFMR at $x \geqslant 5$ originates from substitution of Ni^{2+} for the Mn^{3+} ions, which introduces magnetic dilution of the samples. Also it can be found that, for $T < 230$ K, the MR value of the SB_3 sample is larger than that of the SA_3 sample due to the presence of a larger amount of NiO at the grain boundaries and surfaces in this sample.

Acknowledgments

The authors would like to thank Isfahan University of Technology for supporting this project. Partial support for this project has been provided by Isfahan nanotechnology organization.

References

[1] Jin S, Tiefel T H, Cormack M Mc, Fastnacht R A, Ramesh R and Chen L H 1994 *Science* **264** 413
[2] Okimoto Y, Tomioka Y, Onose Y, Otsuka Y and Tokura Y 1998 *Phys. Rev.* B **57** R 9377
[3] Goodenough J B and Zhou J S 1997 *Nature* **386** 229
[4] Terai T, Kakeshita T, Fukuda T, Saburi T, Takamoto N, Kindo K and Honda M 1998 *Phys. Rev.* B **58** 14908
[5] Zener C 1951 *Phys. Rev.* B **82** 403
[6] Hwang H, Cheong S W, Ong N P and Batlogg B 1996 *Phys. Rev. Lett.* **77** 2041
[7] Gupta A, Gong G Q, Xiao G, Duncombe P R, Lecoear P, Trouilloud P, Wang Y Y, Dravid V P and Sun J Z 1996 *Phys. Rev.* B **54** R 15629
[8] Mathur N D, Burnell G, Isaac S P, Jackson T J, Teo B S, MacManus-Driscoll J L, Cohen L F, Evetts J E and Blamire M G 1997 *Nature* **387** 266
[9] Evetts J E, Blamire M G, Mathur N D, Isaac S P, Teo B S, Cohen L F and MacManus-Driscoll J L 1998 *Phil. Trans. R. Soc. London* A **356** 1593
[10] Guinea F 1998 *Phys. Rev.* B **58** 9212
[11] Dey P and Nath T K 2005 *Appl. Phys. Lett.* **87** 162501
[12] Glaser A and Ziese M 2002 *Phys. Rev.* B **66** 94422
[13] Lopez-Quintela M A, Hueso L E, Rivas J and Rivadulla F 2003 *Nanotechnology* **14** 212
[14] Lamas D G, Caneiro A, Niebieskikwiat D, Sanchez R D, Garcia D and Alascio B 2002 *J. Magn. Magn. Mater.* **241** 207
[15] Balcells Ll, Carrillo A E, Martinez B and Fontcuberta J 1999 *Appl. Phys. Lett.* **74** 4014
[16] Shlyakhtin O A, Shin K H and Oh Y J 2002 *J. Appl. Phys.* **91** 2524
[17] Moshnyaga V *et al* 2003 *Nat. Mater.* **2** 247
[18] Kameli P, Salamati H, Eshraghi M and Mohammadizadeh M R 2005 *J. Appl. Phys.* **98** 43908
[19] Richardson J T and Milligan W O 1956 *Phys. Rev.* **102** 1289
[20] Tiwari S D and Rajeev K P 2006 *Thin Solid Films* **505** 113
[21] Pal S, Bose E, Chaudhuri B K, Yang H D, Neeleshwar S and Chen Y Y 2005 *J. Magn. Magn. Mater.* **293** 872
[22] Gross R, Alff L, Buchner B, Freitag B H, Hofener C, Klein J, Lu Y, Mader W, Philipp J B, Rao M S R, Reutler P, Ritter S, Thienhous S, Uhlenbruck S and Wiedenhorst B 2000 *J. Magn. Magn. Mater.* **211** 150
[23] Vertruyen B, Rulmont A, Cloots R, Ausloos M, Dorbolo S and Vanderbemden P 2002 *Mater. Lett.* **57** 598
[24] Zhang N, Ding W, Zhong W, Xing D and Du Y 1997 *Phys. Rev.* B **56** 8138
[25] Mark Rubinsten J 2000 *J. Appl. Phys.* **87** 5019
[26] Das D, Srivastava C M, Bahadur D, Nigam A K and Malik S K 2004 *J. Phys.: Condens. Matter* **16** 4089
[27] Coey J M, Berkowitz A E, Balcells Ll, Putris F F and Bary A 1998 *Phys. Rev. Lett.* **80** 3815
[28] Garcia-Hernandez M, Guinea F, de Andrés A, Martínez J L, Prieto C and Vázquez L 2000 *Phys. Rev.* B **61** 9549
[29] Sheng P, Abeles B and Arie Y 1973 *Phys. Rev. Lett.* **31** 44
[30] Balcells Ll, Martinez B, Sandiumenege F and Fontcuberta J 2000 *J. Phys.: Condens. Matter* **12** 3013
[31] Gebhardt G R, Roy S and Ali N 1999 *J. Appl. Phys.* **85** 5390
[32] Sun J R, Rao G H and Zhang Y Z 1998 *Appl. Phys. Lett.* **72** 3208
[33] Araujo-Moreira F M, Rajeswari M, Goyal A, Ghosh K, Smolyaninova V, Venkatesan T, Lobb C J and Greene R L 1998 *Appl. Phys. Lett.* **73** 3456